

Flexible Numerical Platform for Electrical Impedance Tomography

A. Fouchard^{*,1,2}, S. Bonnet¹, L. Hervé¹ and O. David²

¹Univ. Grenoble Alpes, CEA, Leti, MINATEC Campus, 17 rue des Martyrs, F-38000 Grenoble, France

²Univ. Grenoble Alpes, Grenoble Institut des Neurosciences, GIN, F-38000 Grenoble, France

*Corresponding author: alexandre.fouchard@centraliens-lyon.net

Abstract: Electrical impedance tomography (EIT) probes biological tissues with low amplitude alternating electrical fields through surface electrodes, and analyzes the medium's response to reconstruct its electrical characteristics. For accurate forward predictions, the complete electrode model (CEM) has to be taken into account. This has motivated the development of custom-built finite element numerical packages. While these codes may be tuned for specific applications, focusing for instance on real-time capabilities, the exploration of new features proves tough both in implementing and debugging. In this paper, the CEM is reviewed, and a means of implementing it into Comsol Multiphysics is proposed. A benchmark is carried out against a standard EIT library in 2D and 3D. Results suggest that the proposed workflow is consistent and efficient. Finally, reconstructions performed using *in vitro* data are presented to point out the completeness of the proposed numerical framework.

Keywords: Electrical impedance tomography (EIT), forward problem, complete electrode model, sensitivity analysis, inverse problem, optimization.

1 Introduction

Electrical impedance tomography (EIT) consists in probing biological tissues with low amplitude alternating electrical fields, through surface source and detector electrodes, and in analyzing the medium's response so as to reconstruct its 3D electrical characteristics [1]–[3]. EIT has been considered for a wide range of clinical applications, the most promising being continuous pulmonary function monitoring [4].

Numerical modeling enables measurement prediction and sensitivity analysis (the forward problem), both required for parameter estimation (the inverse problem). Custom finite element method (FEM) codes are currently the standard ones in the EIT community.

Underlying reasons are twofold. First, the complete electrode model (CEM) must be

employed for accurate forward solving [5]. It is usually presented as non-easily implementable in commercial FEM packages [6], [7]. Second, the sensitivity analysis involves the assembly of a Jacobian matrix, the so-called sensitivity matrix. In its standard form, it requires low-level access (simplex-wise) to products of gradients of shape functions.

This aspect together with the low requirements on the modeling (simple geometry, large regions of conductivity changes, real domain computations, first order shape functions, isotropy) militates for the development of custom numerical packages.

The drawback of such an approach comes from the considerable resources required to address more sophisticated models, able to take into account adaptive high density geometrically-accurate meshes, higher order shape functions, complex domain computations, complicated geometries, anisotropy, and to extend towards multimodality imaging. Then, how to achieve forward modeling remains a challenging task for the EIT community.

In this work, we present a means of implementing the CEM and performing the sensitivity analysis using Comsol Multiphysics. It involves a change from the traditional EIT FEM derivation. Predicted electrical potential distributions are benchmarked against the results of the EIDORS open-source FEM Matlab toolbox [8]. Eventually, parameter estimation using *in vitro* data are shown.

2 Methods

2.1 Complete electrode model

The most accurate formulation of the EIT forward problem is given by the CEM (Figure 1). Following the low frequency quasi-static approximation, it corresponds to the Poisson equation, with Neumann boundary conditions for current injecting electrodes, and Robin conditions to account for both the shunting effect of the conducting electrodes and the contact impedance layer between the electrode and the tissue [5].

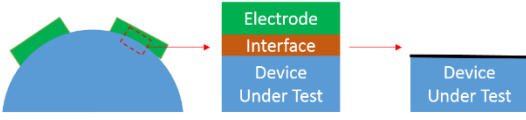


Figure 1. CEM for EIT forward problem: the electrode in itself and the interface are modeled as a boundary condition.

E electrodes $\{E_e\}_{e=1}^E$ are affixed on the surface $\partial\Omega$ of the medium under study Ω . The input data of the forward problem are: the electrical conductivity spatial distribution $\{\sigma(x), x \in \Omega\}$, the contact impedances $\{z_e\}_{e=1}^E$ and the current injection pattern $\mathbf{i}_e = (i_1, \dots, i_E)^T \in \mathbb{R}^E$, of zero mean. The aim is to find the electric potential $\{v(x)\}$ and electrode potentials $\mathbf{v}_e = (v_1, \dots, v_E)^T \in \mathbb{R}^E$, of zero mean, satisfying Eqn. (1), with \mathbf{n} the outgoing normal vector for a closed surface.

$$\left\{ \begin{array}{ll} \nabla \cdot (-\sigma \nabla v) = 0 & \forall x \in \Omega \\ v + z_e \sigma \nabla v \cdot \mathbf{n} = v_e & \forall x \in E_e \\ \int_{E_e} \sigma \nabla v \cdot \mathbf{n} \, d\Gamma = i_e & \forall e = 1 \dots E \\ \sigma \nabla v \cdot \mathbf{n} = 0 & \forall x \in \partial\Omega \setminus \bigcup_{e=1}^E E_e \end{array} \right. \quad (1)$$

Usual derivations of the weak formulation of Eqn. (1) following the Galerkin method lead to a linear system with an augmented stiffness matrix, here called the admittance matrix \mathbf{Y} . For linear shape functions, with the approximated nodal value of v denoted \mathbf{v}_n and N_n nodes, $\mathbf{Y} \in \mathbb{R}^{(N_n+E) \times (N_n+E)}$ is decomposed into 4 blocks, Eqn. (2), in which $\mathbf{Y}_M(\sigma)$ matches the bulk equation derivation and the other blocks translate the handling of boundary conditions, $\mathbf{0}_{N_n}$ being the null vector of specified dimension [9].

$$\mathbf{Y} \begin{bmatrix} \mathbf{v}_n \\ \mathbf{v}_e \end{bmatrix} = \begin{bmatrix} \mathbf{Y}_M(\sigma) + \mathbf{Y}_Z & \mathbf{Y}_W \\ \mathbf{Y}_W^T & \mathbf{Y}_D \end{bmatrix} \begin{bmatrix} \mathbf{v}_n \\ \mathbf{v}_e \end{bmatrix} = \begin{bmatrix} \mathbf{0}_{N_n} \\ \mathbf{i}_e \end{bmatrix} \quad (2)$$

2.2 Data prediction

The approach we present here is quite different in that the discretization of Eqn. (1) does not involve an augmented stiffness matrix. The diffusion partial differential equation is treated as usual in FEM derivations. But, on the contrary of the EIT traditional approach, the CEM boundary

conditions are directly incorporated into the bare admittance matrix.

Indeed, for each electrode e , the boundary conditions boil down to the expression of the normal current density, $-\mathbf{n} \cdot \mathbf{j} = \frac{v_e - v}{z_e}$, with the electrode potential specified as $v_e = \frac{1}{\|E_e\|} \int_{E_e} v \, d\Gamma + z_e i_e$. Combining these relations leads to Eqn. (3), with $\|E_e\|$ the surface of electrode E_e .

$$-\mathbf{n} \cdot \mathbf{j} = \frac{1}{z_e \|E_e\|} \left(\int_{E_e} v \, d\Gamma + z_e i_e - \|E_e\| v \right) \quad (3)$$

Eqn. (3) basically provides a means of coupling both a contact impedance and a current injection in a single Neumann boundary condition.

As for the admittance matrix, Eqn. (3) translates into adding extra elements to the stiffness matrix for implementing the integrate based on quadrature rules. But in this interpretation, its overall size, $\mathbf{Y}^{(\text{com})} \in \mathbb{R}^{N_n \times N_n}$ for linear shape functions, is not modified by taking into account the CEM boundary conditions.

Furthermore, this formulation is compatible with most FEM packages, such as Comsol Multiphysics, in which the implementation is carried out. This allows to use all the numerical methods already available for handling the computations.

The workflow for implementing the proposed scheme in Comsol is the following. Each electrode affixed onto the imaging domain is described geometrically only by a boundary (edge in 2D, surface in 3D), without considering its thickness. It is assigned an integration coupling operator, and two variables for the value of the contact impedance z_e and the flowing current i_e . This allows to specify a normal current density boundary condition to satisfy Eqn. (3), within an electric current physics (AC/DC module). We chose the Pardiso solver to compute the solution with a 10^{-6} relative tolerance.

In EIT, different source positions along with detectors are usually addressed. Comsol built-in parametric sweep allows addressing the different electrode combinations, and the Livelink for Matlab provides flexibility for more intricate source-detector configurations.

2.3 Sensitivity analysis

The sensitivity analysis establishes how each elementary volume in the imaging domain will contribute to the measurements. Following the adjoint approach, the sensitivity of the measurement u_{sd} when source is s and detector d given a variation of the conductivity σ_c of a control volume Ω_c follows Eqn. (4), with I the injected current.

$$\frac{\partial u_{sd}}{\partial \sigma_c} = \frac{-1}{I} \int_{\Omega_c} \nabla v(i^s) \cdot \nabla v(i^d) d\Omega \quad (4)$$

It involves the gradients of electric potential in source and detector configurations, respectively indexed s and d (Figure 2).

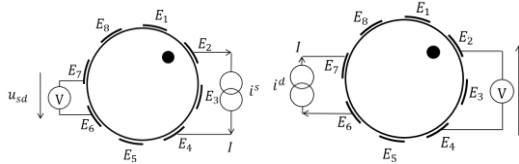


Figure 2. EIT sensitivity analysis: (left) source configuration matching the experimental situation; (right) virtual configuration in which source and detector have been interchanged.

Usually in EIT, Ω_c is chosen to be equal to a simplex in FEM [10]. In Comsol, the evaluation of quantities follows a geometric approach, and gradients of shape functions along mesh elements are *not* accessible and prevent from computing element-wise sensitivity patterns. To overcome this apparent limitation, we shift the focus on nodal-wise sensitivity computations [10], [11].

The control volumes in Eqn. (4) are chosen equal to the Voronoï cells Π_n , which form natural influence domains for each node n in the imaging domain. The electric fields are then approximated by a constant value in each Voronoï cell, the one computed at the mesh vertices. The sensitivity computation then amounts to Eqn. (5), in which $\nabla \mathbf{v}_n(i^s)$ and $\nabla \mathbf{v}_n(i^d)$ are the approximations of the electric field computed respectively in the source and detector configurations.

$$\mathbf{S}_{sd,n}^d = \frac{\partial u_{sd}}{\partial \sigma_n} = \frac{-\|\Pi_n\|}{I} \nabla \mathbf{v}_n(i^s) \cdot \nabla \mathbf{v}_n(i^d) \quad (5)$$

Within Comsol, computing the electric field is quite straightforward and allows sensitivity patterns to be determined for any source-detector configurations.

This defines a forward solver for EIT, as a first component in a Comsol model.

2.4 Parameter estimation

Two options can then be considered for parameter estimation: (i) any EIT inversion algorithm can rely on the forward solver to fit the model to the data, e.g. running studies from Matlab [2]; in particular, the source and detector electric fields can be used directly in a transport setting [12]; (ii) the Comsol Optimization module can perform the inverse problem.

An optimization node is added to the forward problem component to compute the cost function residuals. A second component is added to handle the optimization, through a Levenberg-Marquardt algorithm (LM) (Figure 3).

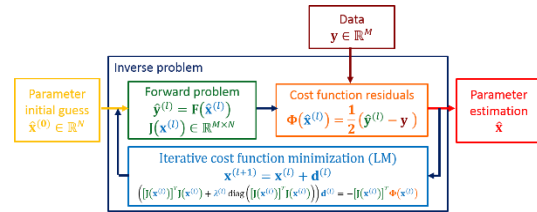


Figure 3. Synopsis of the inverse problem handling within Comsol using the optimization module, to compute the cost function residuals and perform the inversion with a LM algorithm.

2.5 Benchmarking, interfacing with EIDORS

Since most EIT research groups are currently using EIDORS [8] for the computations of the forward problem, we want to compare the performance of this work's derivation of the CEM in a FEM setting along with its Comsol implementation with its EIDORS counterpart on Matlab.

To be able to benchmark both ways of solving the forward problem, the same assumptions have to be considered. Computations are led in the real domain, with 1st order shape functions to approximate the electric potential. Since the conductivity distribution is evaluated by Comsol at Gauss points, the vertices for linear approximation, and EIDORS considers a piecewise constant discretization of σ over mesh elements, the comparison is made on

homogeneous domains (constant σ). Various contact impedance values are considered.

The interfacing with EIDORS involves constructing a corresponding forward model structure fmdl. The Comsol Livelink for Matlab interface enables extracting the mesh information i.e. the vertices, the mesh connectivity, and the electrode pavements from which fmdl can be constructed.

The figure of merit (FoM) used for comparison is the maximum of the relative error over all the nodes or the source-detector configurations. State of the art EIT instrumentation achieves a relative precision of 0.1 % on measurements (electrode potentials), so we expect the numerical modeling to be precise up to a few order of magnitude lower, to avoid bringing further imprecisions into the severely ill-posed EIT inverse problem. Regarding the interior potential used for sensitivity computations, there are currently no known upper limits for the precision of the computation, and the required accuracy remains an open question.

3 Results

3.1 Verification of correct performance

The correctness of the FEM derivation along with its Comsol implementation was first verified. To that end, simulations were performed in two ways.

First, a model in which the analytic is known was considered. A mesh of a cube with two electrodes placed on opposite faces was built, in which the electric field is constant in the perpendicular direction to the electrodes. The size of the cube, the number of elements, the homogeneous conductivity and the contact impedances were varied. The FoM between the Comsol internal potential predictions and the analytical solution was inferior to 10^{-6} in every configuration, and substantially lower when the contact impedances were superior to $10^{-3} \Omega \cdot m^2$. Regarding electrode potentials, the FoM was inferior to 10^{-10} .

Second, the overall behavior of the predictions was studied with a more realistic model. To that end, a 2D numerical phantom was examined, featuring a circular domain of $500 \mu m$ radius with 14 uniformly distributed electrodes (Figure 4).

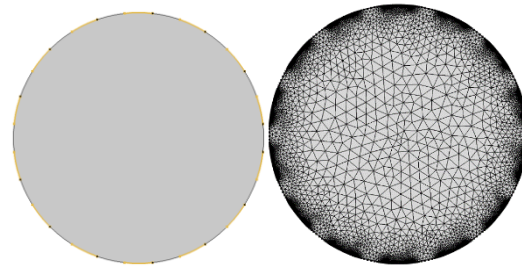


Figure 4. 2D numerical phantom: (left) electrodes are highlighted in yellow; (right) mesh refined at the electrode sites, including 6879 nodes.

Considering a homogeneous conductivity of $1 S \cdot m^{-1}$ and an injected current of 1 mA, the overall behavior of the predictions was epitomized for an adjacent projection (Figure 5).

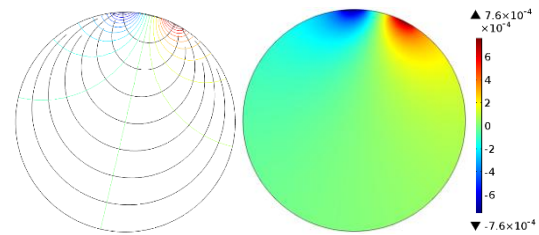


Figure 5. Example of an adjacent projection; left. equipotentials and uniformly distributed current density streamlines; right. potential distribution (V).

A symmetry is observed in the distribution of equipotentials and current density streamlines relative to the 0V equipotential, consistent with the choice of the reference potential in the center of the domain.

The boundary voltage and normal current density were computed for a varying contact impedance z_e of all electrodes from $10^{-6} \Omega \cdot m^2$ to $1 \Omega \cdot m^2$ (Figure 6) (typical values for metallic electrodes in contact with biological tissues).

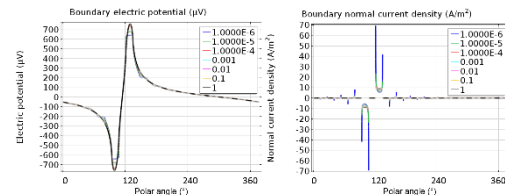


Figure 6. Boundary electric potential (left) and normal current density (right) for varying z_e .

The boundary potential shows a plateau appearance, more pronounced as the contact

impedance decrease. In turn, the normal current density exhibits edge effects.

A zoom on one source electrode (Figure 7), and on one detector electrode (Figure 8) were also plotted, for varying z_e .

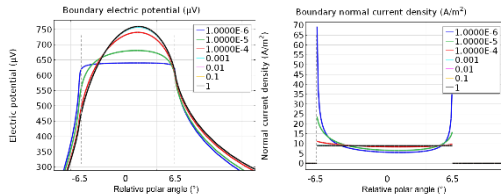


Figure 7. Boundary electric potential (left) and normal current density (right) of a source electrode.

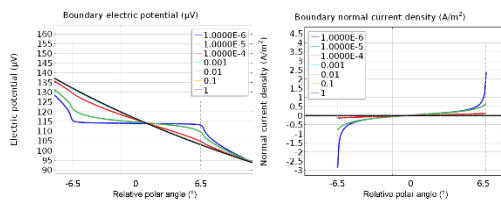


Figure 8. Boundary electric potential (left) and normal current density (right) of a detector electrode.

The potential is especially influenced for high z_e . As for the normal current density, the integrate over a detector is null: no net current flows. Edge effects are particularly noted.

3.2 Benchmarking, 2D and 3D

Considering the 2D numerical phantom depicted above, an example of one admittance matrix computed from the proposed FEM derivation by Comsol was plotted (Figure 9).

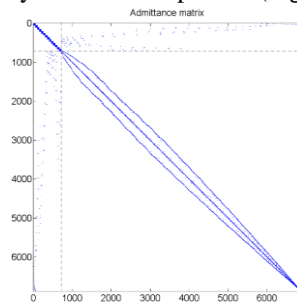


Figure 9. Sparsity plot of an example of a 2D numerical phantom admittance matrix under the proposed FEM derivation, extracted from Comsol.

The internal renumbering puts the nodes belonging to the electrodes in the first position (51 nodes per electrode edges in our case). The taking into account of the CEM boundary conditions

translates into off diagonal extra elements for these nodes.

The Comsol implementation was compared with its EIDORS counterpart for varying contact impedance z_e of all electrodes from $10^{-6} \Omega \cdot m^2$ to $1 \Omega \cdot m^2$. The FoM on nodal potentials was inferior to 10^{-10} and on electrode potentials inferior to 10^{-12} .

The comparison was also led in 3D on a numerical phantom (Figure 10). The same parameter variations were used as in the 2D case.

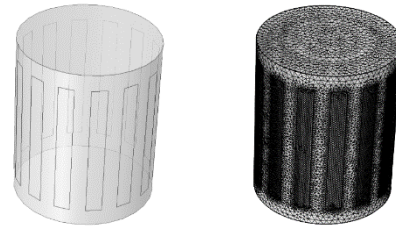


Figure 10. 3D numerical phantom: (left) electrodes are described only by their surface on the domain boundary; (right) relatively coarse mesh used for comparison purposes, using 95054 nodes.

The overall behavior was studied in one adjacent projection (Figure 11).

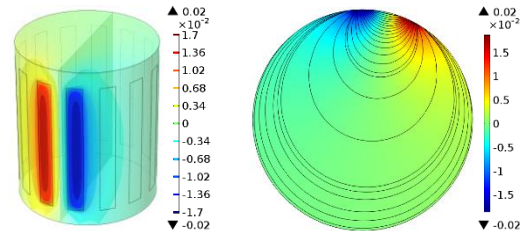


Figure 11. Adjacent projection; left. 3D potential distribution along with 11 iso-potential values (V); right. 2D cross-section in the half-height of the phantom featuring the potential distribution (V) and the amplitude controlled current density streamlines.

The FoM on nodal potentials was inferior to 10^{-4} , but varies strongly with the value of the contact impedance: the FoM lowered by several order of magnitude as the order of magnitude of the contact impedance increased. On the electrode potentials, the FoM was inferior to 10^{-7} in every situation.

Regarding the computational time, considering 14 projections, the overall process of the forward solver (mesh, assembly, solving) took less than 10 s within Comsol for a number of degrees of freedom between 3,000 and 50,000 in

2D. In comparison, EIDORS took 20 s only for the assembly and solving.

In 3D, using 210,725 nodes, EIDORS took 330 s, while Comsol used 550 s to handle all the process. This could be further reduced with computation parallelization in the latter case.

3.3 Parameter estimation, simulated data

Using Comsol optimization module, an absolute reconstruction was performed (Figure 12), using simulated data (inclusion 2 S.m^{-1} versus a background of 1 S.m^{-1} , and an initial guess at background σ).

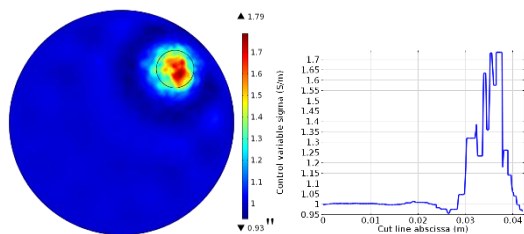


Figure 12. Static inverse problem on synthetic data using Comsol optimization module: the inclusion is correctly recovered in the Levenberg – Marquardt non-linear setting; the expected location is indicated with the black circle; the corresponding profile on the first diagonal shows discontinuities due to the discontinuous Galerkin elements used in the inversion mesh.

The recovery of the inclusion indicates the completeness of the framework proposed to handle both the forward problem and the inverse problem using Comsol.

3.4 Parameter estimation using *in vitro* data

Differential measurements were acquired with a custom-built experimental platform on a saline phantom similar to the one used in the numerical simulations [13]. Inclusions were simulated with conductive metal cylinders of diameter $1/4$ and $1/8$ of phantom diameter.

One step Tikhonov regularized reconstructions were performed [14], with a hyper-parameter chosen by general cross-validation [15] (Figure 13). Sensitivity computations were runned inside Comsol using simplices for mesh elements.

Both inclusions were correctly located inside the imaging domain. Artefacts inherent to the low spatial resolution of EIT were to be seen. The conductivity contrast was not recovered in this case due to the linear inversion algorithm.

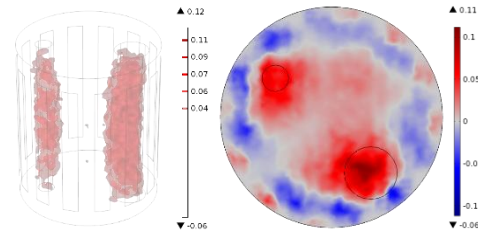


Figure 13. *In vitro* difference reconstructions within Matlab: (left) 3D conductivity iso-values (threshold at $1/4$ of maximum value); (right) cross-section of the conductivity map in the cylinder middle-plane.

4. Discussion

The FEM derivation and corresponding Comsol implementation of the EIT forward problem proposed here enable avoiding the representation of the thickness of electrodes (standard in previous Comsol implementations), and allow benchmarking with other toolboxes.

The validation step shows a consistent overall behavior of the forward solver, with the expected distribution of both current density streamlines and equipotentials. The review of boundary electric potential and normal current density exhibits the interface effects at the electrode – tissue junction, and their fluctuations with varying contact impedances, either on source or detector electrodes.

The implementation compares favorably with EIDORS on 2D and 3D with relative errors on nodal and electrode potential inferior to 10^{-4} as a whole. The main difference between both solvers comes from the way the stiffness matrix, i.e. the admittance matrix, is derived. In this work, no extra dimensions are added to account for the CEM boundary conditions. The electrode potential are deduced during the post-processing in Comsol.

Regarding reconstruction capabilities, both ways to handle the parameter estimation was evaluated: inside Comsol or with external Matlab. Static inversion is effective with Comsol, while one step time difference reconstructions are quite conclusive using the proposed forward solver. The inclusions are located, with artefacts and a poor spatial resolution inherent to EIT. With further regularization to limit the under-determination of the inverse problem, for instance using a dual loosen mesh for inversion, the artefacts might be reduced [10].

5. Conclusion

In this paper, we have presented an implementation of the EIT forward problem in a generalist FEM package while fulfilling the complete electrode model boundary conditions, combining current injection with contact impedance on a single boundary. In the models we studied, we benchmarked our Comsol implementation with the standard matlab EIT library EIDORS.

In this respect, the Comsol Multiphysics environment proves consistent and provides a flexible numerical platform. It can be leveraged to explore more sophisticated models without necessitating numerous developments (higher order shape functions, complex domain computations multiphysics imaging). It appears as a complementary tool alongside custom codes.

The proposed forward solver is generic, and can be adapted to other electromagnetic studies, to compute the potential distribution, e.g. in transcranial direct current stimulation (tDCS), electroencephalography (EEG), and deep brain stimulation (DBS).

References

- [1] D. Holder, *Electrical impedance tomography: methods, history, and applications*. London, UK: Taylor & Francis, 2005.
- [2] J. K. Seo and E. J. Woo, "Electrical Impedance Tomography," in *Nonlinear Inverse Problems in Imaging*, John Wiley & Sons, Ltd, pp. 195–249, 2013.
- [3] A. Fouchard and P. Pham, "Micro-tomographie d'impédance électrique in vivo : une nouvelle modalité d'imagerie ?," *Observatoire des Micro et Nanotechnologies : Avancées, Tendances et Perspectives*, pp. 232 – 235, 2014.
- [4] R. Bayford and A. Tizzard, "Bioimpedance imaging: an overview of potential clinical applications," *Analyst*, vol. 137, no. 20, pp. 4635–4643, 2012.
- [5] E. Somersalo, M. Cheney, and D. Isaacson, "Existence and Uniqueness for Electrode Models for Electric Current Computed Tomography," *SIAM J. Appl. Math.*, vol. 52, no. 4, pp. 1023–1040, 1992.
- [6] W. R. B. Lionheart, "EIT reconstruction algorithms: pitfalls, challenges and recent developments," *Physiol. Meas.*, vol. 25, no. 1, p. 125, 2004.
- [7] W. Zhang and D. Li, "An instrumental electrode model for solving EIT forward problems," *Physiol. Meas.*, vol. 35, no. 10, p. 2001, 2014.
- [8] A. Adler and W. R. B. Lionheart, "Uses and abuses of EIDORS: an extensible software base for EIT," *Physiol. Meas.*, vol. 27, no. 5, p. S25, 2006.
- [9] P. J. Vauhkonen, M. Vauhkonen, T. Savolainen, and J. P. Kaipio, "Three-dimensional electrical impedance tomography based on the complete electrode model," *IEEE Trans. Biomed. Eng.*, vol. 46, no. 9, pp. 1150–1160, 1999.
- [10] A. Fouchard, S. Bonnet, L. Hervé, and O. David, "Méthodes numériques pour le problème direct et l'analyse de sensibilité en tomographie d'impédance électrique," presented at the GRETSI, Lyon, France, 2015.
- [11] A. Fouchard, S. Bonnet, L. Hervé, and O. David, "A current-density conservative nodal framework for EIT," presented at the International Conference on Biomedical Applications of Electrical Impedance Tomography, Neuchâtel, Suisse, 2015.
- [12] A. Fouchard, S. Bonnet, L. Hervé, and O. David, "Inversion without Effective Jacobian Calculations in Electrical Impedance Tomography," in *Journal of Physics: Conference Series*, Institut Farman, Ecole Normale Supérieure de Cachan, Cachan, France, 2014.
- [13] A. Fouchard, A. Noca, S. Bonnet, P. Pham, D. Clarençon, and O. David, "Modular architecture of a Multi-Frequency Electrical Impedance Tomography system: design and implementation," presented at the IEEE EMBC 2014, Chicago, United States, 2014.
- [14] M. Cheney, D. Isaacson, J. C. Newell, S. Simske, and J. Goble, "NOSER: An Algorithm for Solving the Inverse Conductivity Problem," *Int. J. Imaging Syst. Technol.*, 1990.
- [15] P. C. Hansen, "Regularization Tools: A Matlab Package for Analysis and Solution of Discrete Ill-Posed Problems," *Numerical Algorithms*, no. 6, pp. 1-35, 1994.

Acknowledgements

Authors would like to thank instrumentation engineer A. Noca from CEA-LETI for his noteworthy contribution on the design and setting-up of the experimental device. Authors would also like to acknowledge the advices and information provided by Eric Favre and its colleagues from the Comsol support.